High total variation-based method for sparse-view photoacoustic reconstruction

Chen Zhang (张 晨)[1] and Yuanyuan Wang (汪源源)[1,2]

[1]*Department of Electronic Engineering, Fudan University, Shanghai 200433, China*
[2]*Key Laboratory of Medical Imaging Computing and Computer Assisted Intervention, Shanghai 200433, China*
Corresponding author: yywang@fudan.edu.cn

Received June 25, 2014; accepted August 8, 2014; posted online October 28, 2014

We propose a novel method by combining the total variation (TV) with the high-degree TV (HDTV) to improve the reconstruction quality of sparse-view sampling photoacoustic imaging (PAI). A weighing function is adaptively updated in an iterative way to combine the solutions of the TV and HDTV minimizations. The fast iterative shrinkage/thresholding algorithm is implemented to solve both the TV and the HDTV minimizations with better convergence rate. Numerical results demonstrate the superiority and efficiency of the proposed method on sparse-view PAI. *In vitro* experiments also illustrate that the method can be used in practical sparse-view PAI.

OCIS codes: 110.5120, 100.3010, 170.3880, 170.5120.
doi: 10.3788/COL201412.111703.

Photoacoustic imaging (PAI) is a noninvasive medical imaging technique that has a great potential for clinic applications such as early tumor detection[1,2], vessel imaging[3,4], and brain imaging[5]. PAI technique can provide higher contrast[6] and resolution than ultrasound imaging and is more effective for imaging deeper structure compared with pure optical imaging. It combines the strengths of optical and ultrasound imaging[7].

In the practical use of PAI, tissues are illuminated with short laser pulses, which result in the generation of acoustic waves because of the photoacoustic effect. In this letter, we are concerned about the computed tomographic PAI in the imaging mode. The propagated photoacoustic signals are detected by a scanning ultrasound transducer or a transducer array. With the knowledge of these sampling data, the optical absorption deposition within the tissue can be estimated by employing an image reconstruction algorithm.

The key point of imaging quality in PAI is the reconstruction algorithms. Xu *et al.* proposed the filtered back-projection algorithm[8] for PAI, which has been widely used for its convenience. The deconvolution reconstruction algorithm proposed by Zhang *et al.* has specific advantages under the circumstance of limited-angle sampling and heterogeneous acoustic medium[9,10]. The above-mentioned algorithms are the analytical reconstruction methods, which have advantages in the computational cost and implementation convenience. However, the analytical algorithms fail to be effective when the sampling points are sparse and the sparse-view imaging system is very important to reduce data acquaintance time. This drawback limits the applications of the analytical algorithms and impairs their performance.

There also exists PAI system which can image the whole area with one laser exposure. These systems usually have large amount of transducers around the imaging area. With the help of sparse-view PAI reconstruction method, the transducer amount can be reduced. This reduction benefits the system from two main aspects. Firstly, the system is easier to maintain in a lower level of system complexity. Secondly, this reduction can make the data scale much smaller. Besides these two aspects, it is also worth mentioning that it reduces the cost of the system. These aspects are very important for further clinical applications. So it is very important to develop a sparse-view imaging system.

In order to avoid these shortcomings, the model-based iterative algorithms are developed faster in recent years. The iterative algorithms can provide improvement in image quality and noise robustness[11]. Among them, algorithms that adopted the compressed sensing (CS) theory perform best in sparse-view reconstruction[12]. The total variation (TV) method is involved in the CS theory. The TV-based iterative algorithms can recover the images accurately from the sparse sampling data in PAI[13,14]. But it has been shown that the TV-based algorithm sometimes transforms the smooth area into piecewise constants and fails to show some detailed information.

In this letter, we propose a novel algorithm for sparse-view PAI image reconstruction. The algorithm combines the TV minimization with the high-degree TV (HDTV) minimization. Our contributions are threefold. Firstly, we include the HDTV minimization into the PAI reconstruction. This combined method is able to avoid the painting such as artifacts in smooth regions and inherits edge preservation advantage of the standard TV. Secondly, we implement a weighting function to combine the solutions of the TV and the HDTV minimizations. This weighting function is adaptively updated. Thirdly, we extend the fast iterative shrinkage/thresholding

algorithm (FISTA)[15] approach to solve the HDTV minimization. Our numerical simulations confirm that the proposed method is able to reconstruct the image with better quality and more detailed information. *In vitro* experiments illustrate that the method can be used in practical PAI.

Here we focus on two-dimensional PAI. A short pulsed laser is used to illuminate the tissue. Due to the photoacoustic effect, some of the laser energy are absorbed and converted into heat, leading to thermo-elastic expansion and thus acoustic wave generation. Then these photoacoustic signals are detected by ultrasound transducer at different positions in the scanning plane. Based on the assumption that the illumination is spatially uniform and the laser pulse is sufficiently short, the relationship between the detected acoustic signals and the laser absorption distribution can be written as

$$\nabla^2 p(\vec{r},t) - \frac{1}{c^2}\frac{\partial^2 p(\vec{r},t)}{\partial t^2} = -\frac{\mu}{C_{\mathrm{p}}} u(\vec{r}) \cdot \frac{\partial I(t)}{\partial t}, \tag{1}$$

where $p(\vec{r},t)$ is the acoustic pressure measurement at position $\vec{r}$ and time t, c is the speed of sound, C_{p} is the specific heat, μ is the isobaric expansion coefficient, $I(t)$ is the temporal profile of the laser pulse, and $u(\vec{r})$ is the laser absorption distribution.

With the assumption that the speed of sound remains the same, Eq. (1) can be solved as

$$p(\vec{r}_0,t) = \frac{\mu}{4\pi C_{\mathrm{p}}}\frac{\partial}{\partial t}\oiint_{|\vec{r}-\vec{r}_0|=ct}\frac{u(\vec{r})}{t}\mathrm{d}^2\vec{r}, \tag{2}$$

where $\vec{r}_0$ is the position of the ultrasound transducer.

By using the method in Ref. [14], a new variable is defined as

$$f(\vec{r}_0,t) = \frac{4\pi\, C_{\mathrm{p}}}{\mu}\int_0^t p(\vec{r}_0,t)\mathrm{d}t \cdot t. \tag{3}$$

Then Eq. (2) can be converted as

$$f\left(\vec{r}_0,t\right) = \oiint_{|r'-r_0|=ct} u\left(\vec{r}\right)\mathrm{d}^2\vec{r}. \tag{4}$$

In practical imaging, the reconstructed image and the measurements are processed discretely, and the image is reshaped into vectors for convenience. If the size of the reconstructed image $u(\vec{r})$ is X pixels $\times$ Y pixels, then the total pixel number of the reconstructed image $u(\vec{r})$ is N ($N = XY$). After vectorization, the reconstructed image $u(\vec{r})$ becomes a vector $\mathbf{u}$ with the length of N. If the total number of the detection points is Q, the length of measurement in each detection point is M, then Eq. (4) can be expressed as

$$f_i = A_i^{\mathrm{T}} \cdot \mathbf{u} \qquad i = 1,2,\cdots,Q, \tag{5}$$

where f_i is the integration of the $u(\vec{r})$ along the arc that is centered in the ith detection point and with a radius of ct, A_i is the projection matrix of the ith detection point, and T is the transpose operation of a matrix.

It is reported[14] that the image can be accurately recovered from the sparse sampling data by minimizing the TV value. The TV value is defined as

$$\mathrm{TV}(u) = \sum_{i,j}\left|\vec{\nabla} u\right| = \sum_{i,j}\sqrt{(u_{i,j}-u_{i-1,j})^2 + (u_{i,j}-u_{i,j-1})^2}. \tag{6}$$

Using TV values to reconstruct the image can be expressed as the following optimization problem:

$$\min_u\left\{a\cdot \mathrm{TV}(u) + \frac{1}{2}\left|A\mathbf{u}-f\right|_2^2\right\}. \tag{7}$$

An iterative algorithm is implemented to solve this problem. The iteration step consists of two parts, the residual corrections of all sampling points and the TV minimization by the FISTA[15] method. They are carried out repeatedly to accomplish the image reconstruction. The iteration can be summarized as follows:

1. Calculate the residual corrections $\Delta\mathbf{u}$ using

$$\Delta\mathbf{u} = \frac{A_i}{\left\|A_i\right\|^2}(f_i - A_i\cdot\mathbf{u}) \quad i = 1,2,3,\ldots,Q. \tag{8}$$

2. Transform the vector $\Delta\mathbf{u}$ into the image domain to get the residual corrections image Δu, update the reconstructed image by $u_{\mathrm{new}} = u - \Delta u$.
3. After completing the corrections of all sampling points, the updated image u_{new} is processed by the FISTA method for TV minimization.

This iteration is carried out repeatedly to accomplish the image reconstruction result u_1.

But it has also been shown that the TV-based algorithms reconstructed the smooth area image with piecewise constants and sometimes lose some detailed information. To overcome this spurious effect, we involve the HDTV into the reconstruction. The HDTV value is defined as

$$\mathrm{HDTV}(u) = \sum_{i,j}\sqrt{(u_{i,j}-2u_{i-1,j}+u_{i-2,j})^2 + (u_{i,j}-2u_{i,j-1}+u_{i,j-2})^2}. \tag{9}$$

Using the HDTV values to reconstruct the image can be expressed as the following optimization problem:

$$\min_u\left\{a\cdot \mathrm{HDTV}(u) + \frac{1}{2}\left|A\mathbf{u}-f\right|_2^2\right\}. \tag{10}$$

An iterative algorithm similar to the optimization Eq. (7) is implemented to solve the problem. Here we propose the FISTA method for HDTV minimization.

Firstly we give some notations in order.

(W, Q) is the matrix pair where $W \in R^{(X-2)\cdot Y}$ and $Q \in R^{X\cdot(Y-2)}$ that satisfy

$$w_{i,j}^2 + q_{i,j}^2 \le 1,$$

where $w_{i,j}$ and $q_{i,j}$ are the elements in matrices W and Q.

L is a linear operation defined by

$$L(P,\mathrm{Q})_{i,j} = w_{i,j} + q_{i,j} - 2w_{i+1,j} - 2q_{i,j+1} + w_{i+2,j} + q_{i,j+2}.$$

L^{T} is a linear operation defined by

$$L^T(u) = (W,Q),$$

where $W \in R^{(X-2)\cdot Y}$ and $Q \in R^{X\cdot(Y-2)}$ are matrices defined by

$$w_{i,j} = u_{i,j} - 2u_{i-1,j} + u_{i-2,j},$$

$$q_{i,j} = u_{i,j} - 2u_{i,j-1} + u_{i,j-2}.$$

With these notations, we can transform Eq. (9) as

$$\max_{P,Q} \min_{u} \left\{ a \cdot Tr(L(P,Q)^T \cdot u) + \frac{1}{2} \left| A\boldsymbol{u} - f \right|_2^2 \right\}. \quad (11)$$

The dual problem described in Eq. (11) is in the same form of the FISTA dual problem. We can implement the FISTA algorithm to the HDTV minimization by using our new notations. By using the same iteration process to solve Eq. (7) we can accomplish the reconstructed image u_2.

We use a convex combination to generate a new solution that contains the best from each of these two methods. It is defined as

$$u = \theta \cdot u_1 + (1-\theta) \cdot u_2, \quad (12)$$

where θ is the weighting function that can be found adaptively between the iterations. The weighting function is updated according to

$$\theta = \begin{cases} 1 & \text{if} \quad \left|\nabla\omega\right| \geq th, \\ \frac{1}{2}\cos\left(\frac{2\pi\left|\nabla u\right|}{th}\right) + \frac{1}{2} & \text{else.} \end{cases} \quad (13)$$

As a result, the combined HDTV and TV algorithm, which we will refer to as the HDTV-FISTA algorithm, is summarized as follows:

1. Initialization: the initialization reconstructed has to be zero matrix.
2. Use the FISTA algorithm for TV minimization to get reconstructed image u_1.
3. Use the FISTA algorithm for HDTV minimization to get reconstructed image u_2.
4. Combine u_1 and u_2 by Eq. (12).
5. Update θ by Eq. (13).
6. When the exiting criterion is met, end the iterations. Otherwise return to step (2).

Here we present the simulation results obtained from the proposed HDTV-FISTA method to verify the effectiveness on PAI. The simulation platform is that of Matlab v7.14 on a PC with 3.07 GHz Intel Xeon processor (only 1 core is used in simulation) and 32 GB memory. The speed of sound is set to be consistent in the simulation as 1500 m/s.

In the simulation, we choose the FORBILD phantom to be the initial optical absorption distribution image. The phantom is shown in Fig. 1. The measurements from the phantom are generated by using Eq. (2). The size of the phantom is 89.6×89.6 (mm) and the radius of the scanning circle is 42 mm. The reconstructed image is 128×128 pixels. We simulate the situations of 90, 60, and 30 sampling angles, which cover a full 360° angular range.

In this simulation, the performance of HDTV-FISTA is compared with the L_1-norm[12] and the TV gradient descent (TV-GD)[14] algorithms. The iterations steps are all set to be 10. The parameter th is set to be 0.2. The reconstructed images by L_1-norm, TV-GD, and HDTV-FISTA algorithms are shown in Fig. 2.

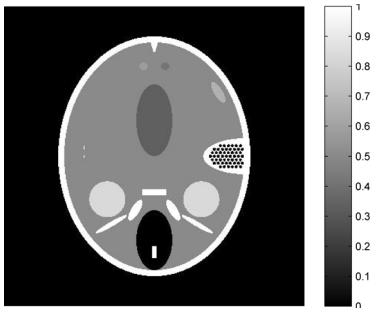

Fig. 1. FORBILD phantom.

It is shown in the first column of Fig. 2 that all the algorithms can reconstruct the accurate image when the sampling data are sufficient. When the sampling angles get sparse during the simulation, the L_1-norm method struggles to depress the noise and the image quality is severely affected. The TV-GD algorithm is the closest to the HDTV-FISTA in image quality. When it comes to the extreme sparse sampling angles (30 views), the painting such as staircase artifacts emerges in the smooth regions of the TV-GD reconstruction result. Also the reconstruction result is far from accurate in the low contrast regions in the top and left of the phantom. Meanwhile the HDTV-FISTA results are not affected in these regions. The decreasing of the sampling views does not substantially affect the quality of HDTV-FISTA reconstruction.

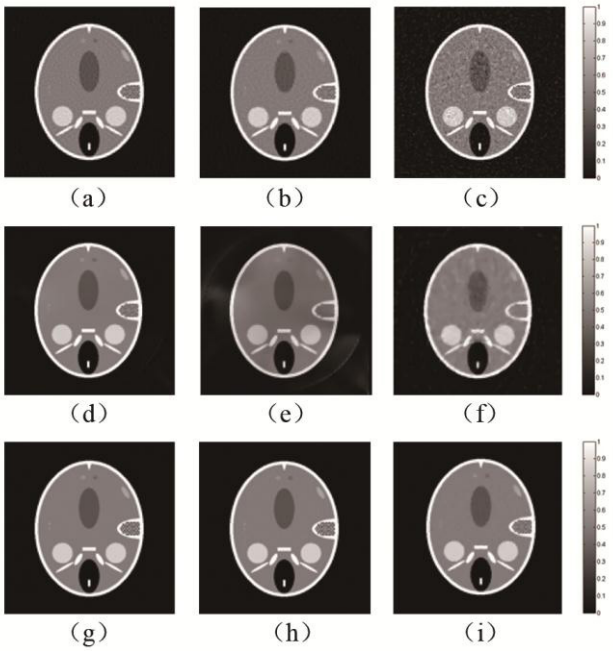

Fig. 2. Images in rows reconstructed by (a–c) L_1-norm, (d–f) TV-GD, and (g–i) HDTV-FISTA algorithms, respectively. Images in columns refer to the results from 90-, 60-, and 30-view, respectively.

Table 1. PSNRs (dB)/MSE of Reconstructed Images of FORBILD Phantom

PSNRs (dB)/MSE	90-view	60-view	30-view
L_1-norm	28.68/0.136	26.53/0.222	20.67/0.851
TV-GD	31.75/0.067	29.68/0.108	26.63/0.217
HDTV-FISTA	40.37/0.009	39.12/0.012	38.15/0.015

We calculate the peak signal-to-noise ratio (PSNR) and mean-square error (MSE) of the reconstructed images with the original FORBILD images as standard to evaluate the above-mentioned methods. The quantitative results are shown in Table 1. Among all the three CS-based algorithms, the PSNRs of the images reconstructed by the HDTV-FISTA are the highest. We continuously decrease sampling point amount in order to find the limit density of the sampling points. In this simulation, the image is acceptable when its PSNR can reach 30 dB. It is revealed from the simulation that the density of the transducer can be reduced to 15 for HDTV-FISTA algorithm. The comparison of the visual sensation and the PSNR value demonstrates that the HDTV-FISTA is the most accurate and stable algorithm in sparse-view PAI.

We also scan the imaging area with un-equal angle step to test the universality of our algorithm. The simulation setup and the result are shown in Fig. 3. As can be seen from Fig. 3, the reconstruction result can still maintain a very high quality.

We study the convergence rate of the proposed method through the simulation. The TV-GD algorithm is reported as an efficient and stable iterative algorithm in PAI. Its reconstruction results are closest to the proposed algorithm in image quality. Here we compare it with the HDTV-FISTA algorithm. The sampling view is 30. It is reported that the FISTA-based methods have a global rate of convergence which is significantly better than currently known gradient-based methods. To explore the accuracy obtained by these two algorithms, we use a parameter that shows the difference between the reconstructed image and the original phantom image. The parameter d is defined as

$$d = \left(\frac{\sum_{i=1}^{X} \sum_{j=1}^{Y} (u(i,j) - t(i,j))^2}{\sum_{i=1}^{X} \sum_{j=1}^{Y} t(i,j)^2} \right)^{1/2}, \tag{14}$$

where u is the reconstructed image and t is the original image. The size of the image is $X \times Y$. The simulation result is shown in Fig. 4.

The x-axis shows the value of difference and the y-axis shows the iteration times. The line '•—' refers to the TV-GD algorithm and the line 'o—' represents the HDTV-FISTA algorithm. Clearly, the HDTV-FISTA reaches greater accuracies than the image reconstructed by the TV-GD. Moreover, the function value d reached by the TV-GD after eight iterations is already obtained by the HDTV-FISTA after three iterations. It can be surmised that the convergence rate of the HDTV-FISTA algorithm is faster than that of the TV-GD algorithm.

We also verify the HDTV-FISTA algorithm through the *in vitro* experiment. The PAI system is illustrated in Fig. 5(a). An Nd:YAG laser generator (Continuum, Surelite I) with a wavelength of 532 nm and a repetition rate of 10 Hz is used. An ultrasound immersion transducer (Panametric, V383-SU) with a central frequency of 3.5 MHz and a bandwidth of 3.5 MHz is used to receive the photoacoustic signals. The signals are amplified by the pulse receiver (Panamertric, 5900PR) and sampled by the oscilloscope (Agilent, 54622D).

During the experiment, we use gelatin cylinder to make the imaging tissue, as shown in Fig. 5(b). The radius of the phantom is 25 mm. The phantom is made by three rubber bars with diameter of 1 mm that embedded as the optical absorbers. In the experiment, the transducer circularly scans around the imaging tissue with a radius of 42 mm. The angular step

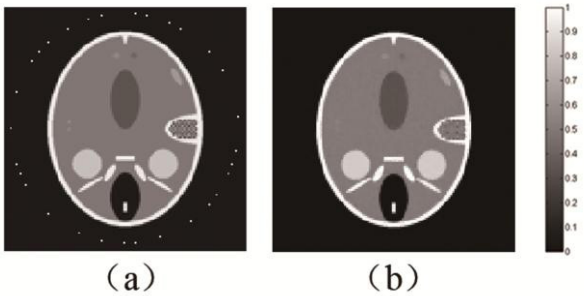

Fig. 3. Un-equal angle step scanning: (a) projection setup and (b) reconstruction result.

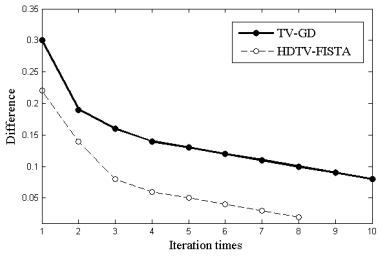

Fig. 4. Difference between the reconstructed images and the original phantom image versus the iteration number.

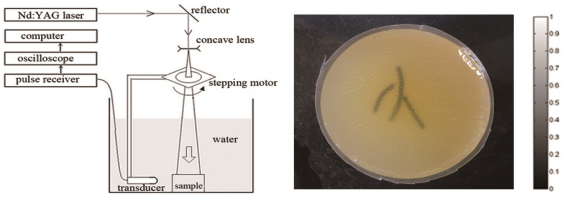

Fig. 5.(a) Scheme of the experiment platform. (b) Photo of the imaging samples.

is set to be 4° and 12°. The sampling frequency of the oscilloscope is set to 16.67 MHz.

The images are reconstructed by the L_1-norm, the TV-GD, and the HDTV-FISTA algorithms. The reconstructed images are shown in Fig. 6. We can find out from the first row of Fig. 6 that these algorithms are all effective in the sufficient data condition. When the sampling view is sparse, it is shown in the image that the artifacts emerge and the quality is severely affected in the L_1-norm and the TV-GD algorithm. Meanwhile, it is shown that the HDTV-FISTA algorithm outperforms the other two algorithms in image contrast and noise suppression. The structure of the phantom is clear and the background noise is well suppressed. The comparison indicates that the HDTV-FISTA method has a better performance in the situation of sparse-view

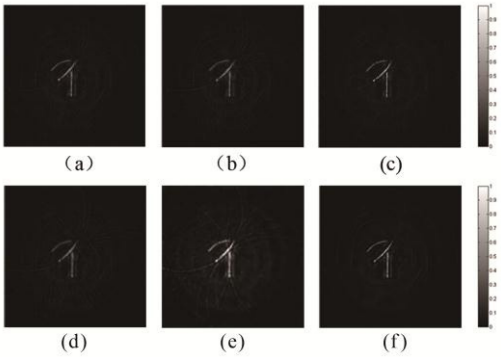

Fig. 6. Reconstructed images of rubber sample. The first row is 90-view and the second is 30-view. Images from the left to right refer to reconstructed by the L_1-norm, the TV-GD, and the HDTV-FISTA algorithm, respectively.

sampling data, which contributes to the reduction of the scanning time in practical use.

In conclusion, we propose an iterative method for the PAI reconstruction based on TV and HDTV minimizations. The FISTA method is implemented to provide better rate of convergence. Through the numerical simulations and *in vitro* experiment, the proposed method is able to reconstruct the image with better quality and can be used in practical sparse-view PAI.

This work was supported by the National Natural Science Foundation of China (Nos. 61271071 and 11228411), the National Key Technology R&D Program of China (No. 2012BAI13B02), and the Specialized Research Fund for the Doctoral Program of Higher Education of China (No. 20110071110017).

References

1. B. Guo, J. Li, H. Zrnuda, and M. Sheplak, IEEE Trans. Biomed. Eng. **54,** 2000 (2007).
2. M. Pramanik, G. Ku, C. Li, and L. V. Wang, Med. Phys. **35,** 2218 (2008).
3. E. Z. Zhang, J. G. Laufer, R. B. Pedley, and P. C. Beard, Phys. Med. Biol. **54,** 1035 (2009).
4. J. J. Niederhauser, M. Jaeger, R. Lemor, P. Weber, and M. Frenz, IEEE Trans. Med. Imaging **24,** 436 (2005).
5. A. de la Zerda, Y. M. Paulus, R. Teed, S. Bodapati, Y. Dollberg, B. T. Khuri-Yakub, M. S. Blumenkranz, D. M. Moshfeghi, and S. S. Gambhir, Opt. Lett. **35,** 270 (2010).
6. Y. Gao, Y. Deng, X. Tong, H. Wang, Z. Deng, X. Yang, Y. Liu, H. Gong, and Q. Luo, Chin. Opt. Lett. **10,** 061101 (2012).
7. S. Ye, J. Yang, J. Xi, Q. Ren, and C. Li, Chin. Opt. Lett. **10,** 121701 (2012).
8. M. H. Xu and L. H. V. Wang, Med. Phys. **29,** 1661 (2002).
9. C. Zhang and Y. Wang, J. Opt. Soc. Am. A Opt. Image Sci. Vis. **25,** 2436 (2008).
10. C. Zhang, C. Li, and L. V. Wang, IEEE Photon. J. **2,** 57 (2010).
11. G. Paltauf, J. A. Viator, S. A. Prahl, and S. L. Jacques, J Acoust. Soc. Am. **112,** 1536 (2002).
12. Z. Guo, C. Li, L. Song, and L. V. Wang, J. Biomed. Opt. **15,** 021311 (2010).
13. K. Wang, R. Su, A. A. Oraevsky, and M. A. Anastasio, Phys. Med. Biol. **57,** 5399 (2012).
14. Y. Zhang, Y. Wang, and C. Zhang, Ultrasonics **52,** 1046 (2012).
15. A. Beck and M. Teboulle, IEEE Trans. Image Process. **18,** 2419 (2009).